Optimizing MRD Inlet Performance through Disk Geometry Modification at Supersonic Flow Regime

Jayanta Sinha
Research Scholar
Amity Institute of Aerospace Engineering
Amity University Uttar Pradesh Noida
India

Sanjay Singh
Professor
Amity Institute of Aerospace Engineering
Amity University Uttar Pradesh Noida
India

Om Prakash
Professor
Department of Aerospace Engineering
University of Petroleum and Energy Studies
Dehradun
India

This study investigates the influence of disk edge geometry on the flow physics and pressure characteristics of a Multi-Row Disk Inlet Device (MRDID) operating at Mach 2 within the open cavity regime (L/D = 1). *A detailed parametric analysis was conducted using 2D axisymmetric RANS simulations with the SST* k-ω *turbulence model and second-order MUSCL discretization, supported by supersonic wind tunnel experi–ments for validation. Two baseline geometries, the Flat Tip Disk (FTD) and Sharp Tip Disk (STD), were examined to understand the role of rear-wall stagnation and cavity shock interaction. Results show that FTD produces higher peak pressure ratios, compression, and drag due to a strong stagnation zone at the cavity rear wall, whereas STD reduces stagnation severity through its inclined surface. To explore passive flow control, two modified geometries—Rear Chamfered Tip Disk (RCTD) and Front Chamfered Tip Disk (FCTD)—were introduced. Rear chamfering improves wake recovery and reduces recompression shocks, while front chamfering transforms the detached bow shock into an attached oblique shock, significantly lowering peak pressure. The study establishes disk edge shaping as a critical passive design parameter for optimizing MRD inlet performance.*

Keywords: *Multi-Row Disk Intake, Supersonic Intake Design, Mach Number, Disk geometry, Passive Flow modifications, Numerical Simulation, Cavity flow*

1. INTRODUCTION

The aerodynamic design of supersonic inlets is funda–mentally governed by the principles of compressible flow, where the deceleration and compression of high-speed air are achieved through controlled shock systems prior to entry into the engine compressor. Classical gas-dynamic formulations describe how oblique and normal shocks can be arranged within diffusers to achieve ma–ximum pressure recovery with minimum total pressure loss [1]. Detailed treatments of intake aerodynamics further explain how inlet geometry determines shock formation, flow turning, and overall diffuser efficiency in practical configurations [2]. These principles become even more demanding in high-speed and hypersonic propulsion systems, where precise shock control is es–sential for engine operability across a wide Mach range [3]. Comprehensive discussions on scramjet and high-Mach propulsion further highlight the stringent require–ments imposed on inlet performance under extreme flow conditions [4].

Early analytical and experimental investigations into supersonic diffusers established the theoretical limits of pressure recovery and emphasized the importance of correct shock positioning in inlet passages [5]. Subs–equent studies on supersonic diffuser starting charac–teristics provided deeper understanding of how back pressure and geometry influence shock stability within the inlet [6]. As research progressed, the detrimental effects of shock–boundary layer interaction in super–sonic intakes were recognized, showing how separation and pressure loss occur due to improper shock mana–gement [7]. Extensive reviews on shock-wave/ boundary-layer interactions consolidated the understan–ding of separation mechanisms responsible for inlet inefficiencies [8].

Parallel to inlet studies, investigations into cavity flows revealed important flow features relevant to pas–sive shock control. Experiments on cavity flow oscil–lations demonstrated the presence of strong pressure fluctuations and shear layer dynamics in supersonic streams [9]. Axisymmetric cavity studies by Mohri and Hiller provided a systematic classification of cavities based on the length-to-depth (L/D) ratio, identifying open, transitional, and closed cavity regimes with dis–tinctly different flow behavior [10]. Building upon such cavity flow principles, Kobayashi proposed the Multi-Row Disk Inlet Device (MRDID) as a novel fixed-geometry inlet concept using multiple disks arranged along the centerbody [11]. Further studies by Kobayashi and co-workers showed how these disks generate a series of compression and expansion waves while forming cavities that act as passive flow control elements [12].

Subsequent experimental investigations into open cavity flows in supersonic regimes validated the rele–vance of L/D-based cavity classification for internal

Received: January 2026, Accepted: April 2026
Correspondence to: Mr. Jayanta Sinha, Amity Institute of Aerospace Engineering Amity University Uttar Pradesh Sector 125, Noida, UP-201313, India
E-mail: jsinha1987@gmail.com
doi: 10.5937/fme2602380S

high-speed flows and demonstrated its influence on pressure oscillation characteristics [13]. Additional studies quantified the effect of cavity L/D ratio on wall pressure fluctuations and flow stability in supersonic internal passages [14]. Collaborative studies on axisymmetric cavities further reinforced the importance of cavity geometry in governing shock interaction and oscillatory behavior [15]. Advanced optical visualization methods such as schlieren and shadowgraph techniques have been instrumental in revealing these shock and cavity interactions in experimental studies [16].

Fundamental gas-dynamic texts continue to provide the theoretical basis for interpreting shock reflections, expansions, and boundary layer interactions in such internal flows [17]. Classical treatments of supersonic aerodynamics alsodescribe how diffuser geometry influences shock patterns and pressure recovery [18]. Modern investigations into supersonic inlet design for high-speed vehicles emphasize the need for robust geometries capable of maintaining performance across varying flight conditions [19]. Detailed studies on external compression inlet configurations further illustrate how inlet shape governs shock attachment and pressure distribution [20].

Despite these advances, fixed-geometry inlets operating under off-design conditions are susceptible to low-frequency oscillatory instabilities known as inlet "buzz," which arise due to shock motion within the duct [21]. To mitigate such effects, passive control techniques such as cavities and recessed geometries have been explored for stabilizing shock–boundary layer interactions without mechanical complexity [22]. Investigations into pressure oscillations and tonal behavior in cavity flows provide further understanding of how shear layer dynamics influence internal flow stability [23]. Studies on inlet flow distortion additionally demonstrate how such instabilities directly affect engine performance and operability [24].

Variable geometry solutions, such as those implemented in the Concorde inlet system with adjustable ramps, demonstrated how adaptable geometries can effectively manage internal shock structures during supersonic cruise [25]. However, the mechanical complexity of such systems continues to motivate the exploration of simpler passive alternatives.

In this context, the MRDID concept offers a promising fixed-geometry approach where cavities formed between disks act as passive flow control elements. While earlier studies have demonstrated its potential in improving inlet performance [6,14,26], limited attention has been given to the influence of disk geometry, edge profile, size, and spacing on the resulting shock structure and wall pressure distribution. Since the cavities formed between disks fall within the open cavity regime defined by L/D criteria, a systematic study of disk geometry becomes essential. The present work therefore investigates the shock structures produced by disks of varying geometries at Mach 2 and examines how passive geometric modification influences the open cavity flow field, building directly upon the established understanding of compressible flow, inlet aerodynamics, shock interactions, cavity physics, and MRDID research documented in the literature.

Figure 1 shown below represents all the important flow parameters for the Open cavity structure.

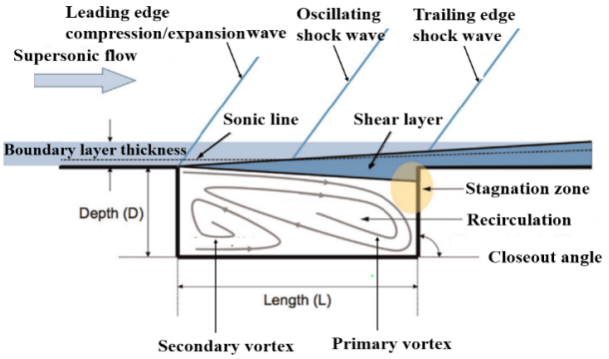

Figure 1. Basic open cavity structure

This work is directly applicable to the design of fixed-geometry supersonic inlets for UAVs, missiles, and ramjet/scramjet systems, offering a simpler alternative to variable-geometry designs. The study demonstrates that disk edge geometry can act as an effective passive flow control mechanism. Scientifically, the work provides the first systematic analysis of disk edge shaping in MRDID within the open cavity regime. The combined CFD–experimental validation strengthens its reliability and practical engineering relevance.

Existing studies on MRDID and supersonic cavity flows primarily focus on disk spacing, cavity aspect ratio, or active/passive control methods, with limited attention to disk edge geometry. Additionally, the influence of edge shaping on shock–cavity interaction and pressure characteristics remains insufficiently explored. The novelty of the present work is that it addresses this gap by systematically investigating disk edge modifications and their impact on flow physics, thereby establishing its novelty and scientific contribution.

Another aspect of novelty of this paperlies in the fact that certain literature hasdiscussed the disks which have conventional flat outer circumference but no research has been undertaken to understand the effect of shape of the disks. Also, there are few papers which talks about the passive modification of the cavity structure by rear wall or front wall inclinations but there is no data which talks about the implementation of the passive modi–fication of the disks on the MRDID. So, the importance of the current research and the novelty isthat, it has reported two important issues – Firstly, the analysis of the Disk shape and its selection from the Aerodynamics and structural point of view. It has been reported in the first part of the paper. Secondly, the effect of the passive modification of the disk shape and its implementation in the MRDID. It has been addressed in the second part of the paper. All these cases have been analysed using Steady simulations. Peak Pressure ratio and the Drag coefficient are the parameters of analysis and comparison.

2. GEOMETRY DESIGN

The geometry of the MRDID used for numerical analysis is obtained through multiple iterations based on the literature provided bySinha et al [6,14,26] and Kobayashi et al. [11-12]. Figure 2 gives the parametric

idea of the MRDID and figure represents the self-designed MRDID already published by Sinha et al.

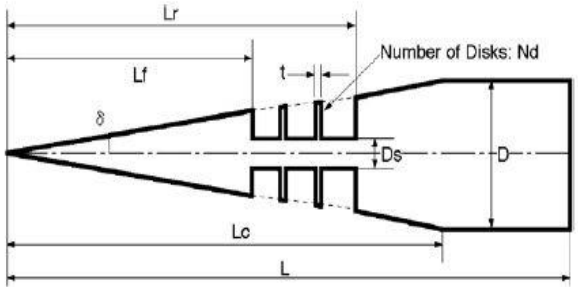

Figure 2. Schematic diagram of MRD

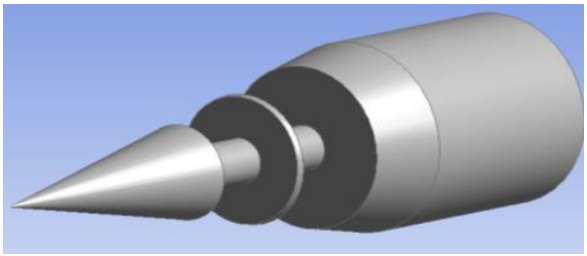

Figure 3. Self-designed MRDID

Self-designed MRDID has been subjected to all the analysis reported in this paper. Based on the geometry of the MRDID, disk has been selected and the disk spacing is finalized. Disk spacing has been chosen such that it always remainswithin the open cavity domain and under no condition it extends beyond L/D =3.

Depending on the iterative study on the cavity flow features over different cavity aspect ratio, following CAD designs were made as shown in Figure 4 and 5. Further, experimental models were developed as shown in Figure 6 and 7. Figure 4 and 5 show the disk geo–metry as the Flat tip disk and the sharp tip disk res–pectively.

Figure 4. CAD Model of the FTD

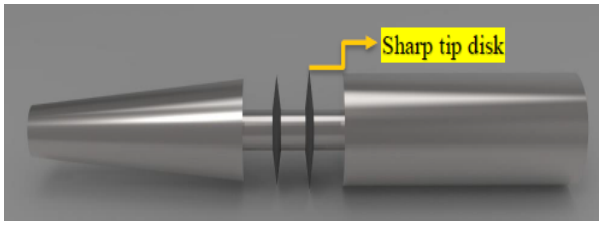

Figure 5. CAD Model of the STD

Figure 6. Experimental model for STD

Figure 7. Experimental model for FTD

In the further discussions, they will be referred as FTD and STD for easy communication. Models shown in Figure 4 and 5 were used for Simulation purpose and those inFigure 6 and 7 were used for experimental purpose.

3. NUMERICAL MODELLING

For the purpose of carrying out the numerical simu–lations, validated steady state, two-dimensional (2D), axisymmetric, implicitReynolds-Averaged Navier–Sto–kes (RANS) equations were solved using a second-order MUSCL scheme for spatial discretization, coupled with the SST k–ω turbulence model. This turbulence model provides the advantages of both the k-ω model (accurate near-wall treatment) and the k-ε model (robustness in the free stream).SST also switches between wall func–tions and the viscous sublayer treatment as necessary.

The MUSCL scheme is widely used for solving hyperbolic partial differential equations like the comp–ressible Navier-Stokes equations. It is effective for capturing shocks and discontinuities, which are com–mon in supersonic flows, such as those encountered in a multi-row disk supersonic inlet.So, in this case, we aim to simulate the supersonic flow over a multi-row disk inlet using the MUSCL scheme. This setup will analyze the flow characteristics such as shocks, expansion wa–ves, and overall aerodynamic performance of the inlet.

The MUSCL scheme extends the first-order Godu–nov scheme by using piecewise linear reconstructions to achieve second-order accuracy in space. This is cri–tical for accurately capturing the complex flow pheno–mena like shocks and expansions seen in supersonic inlets.

3.1 Implementation of MUSCL scheme

i. Performed linear reconstruction of the conserved variables like density, momentum and energy at the cell interfaces. The reconstructed values ensure higher order accuracy.
ii. Minmod slope limiters have been applied to avoid abrupt oscillations near the shocks.
iii. AUSM based Rieman Solver has been used at the cellinterface to compute the fluxes.
iv. The conserved variables will be updated after each fluxed are obtained from the Rieman Solver. These updates will be done n time stepping. R-K method is used for this case.
v. CFL condition has been used for the stability and the time step for the simulation is calculated using the formula given below:

$$\Delta t = \frac{CFL}{MAX\left(\frac{u+c}{\Delta x}, \frac{v+c}{\Delta y}\right)} \tag{1}$$

3.2 Governing equations

The flow field is modelled by solving the steady, comp–ressible Reynolds-Averaged Navier–Stokes (RANS) equations in an axisymmetric framework. Turbulence closure is achieved using the *k–ω* Shear Stress Trans–port (SST) model, which employs a blending function to combine the near-wall accuracy of the *k–ω* formulation with the free-stream independence of the *k–ε* model. The SST model incorporates a limiter on turbulent eddy viscosity and accounts for the transport of turbulent shear stress, enabling improved prediction of flow separation under adverse pressure gradients.

i. Compressible RANS Equation

a) Continuity Equation:

$$\frac{\partial \rho}{\partial t}+\frac{\partial\left(\rho u_i\right)}{\partial x_i}=0 \tag{2}$$

b) Momentum Equation:

$$\frac{\partial\left(\rho u_i\right)}{\partial t}+\frac{\partial\left(\rho u_i u_j\right)}{\partial x_j}=-\frac{\partial P}{\partial x_i}+\frac{\partial\left(\tau_{ij}-\overline{\rho u_i' u_j}\right)}{\partial x_j} \tag{3}$$

c) Energy Equation:

$$\frac{\partial(\rho E)}{\partial t}+\frac{\partial\left[u_i(\rho E+P)\right]}{\partial x_i}=-\frac{\partial P}{\partial x_i}\left[k_{eff}\frac{\partial T}{\partial x_i}+u_j\left(\tau_{ij}\right)_{eff}\right] \tag{4}$$

3.2.1 Constitutive Relation

a) Viscous Stress Tensor

$$\tau_{ij}=\mu\left(\frac{\partial u_i}{\partial x_i}+\frac{\partial u_j}{\partial x_i}-\frac{2}{3}\delta_{ij}\frac{\partial u_k}{\partial x_k}\right) \tag{5}$$

b) Reynolds Stress (Boussinesq Approximation)

$$-\overline{\rho u_i' u_j'}=\mu_t\left(\frac{\partial u_i}{\partial x_j}+\frac{\partial u_j}{\partial x_i}\right)-\frac{2}{3}\rho k\delta_{ij} \tag{6}$$

c) Total Energy

$$\mathrm{E}=\mathrm{h}-\frac{P}{\rho}+\frac{1}{2}u_i u_i \tag{7}$$

d) Equation of State (Perfect Gas)

$$\mathrm{P}=\rho\mathrm{RT} \tag{8}$$

3.2.2 Turbulence Model: k–ω SST

a) Turbulent Kinetic Energy Equation (K)

$$\frac{\partial(\rho k)}{\partial t}+\frac{\partial\left(\rho k u_i\right)}{\partial x_i}=P_k-\beta^*\rho k\omega+\frac{\partial}{\partial x_i}\left[\left(\mu\sigma_k\mu_t\right)\frac{\partial k}{\partial x_i}\right] \tag{9}$$

b) Specific Dissipation Rate equation (ω)

$$\frac{\partial(\rho\omega)}{\partial t}+\frac{\partial\left(\rho\omega u_i\right)}{\partial x_i}=\alpha\frac{\omega}{k}P_k-\beta\rho\omega^2+$$
$$+\frac{\partial}{\partial x_i}\left[\left(\mu+\sigma_\omega\mu_t\right)\frac{\partial\omega}{\partial x_i}\right]+2\left(1-F_1\right)\rho\sigma_{\omega 2}\left(1/\omega\right)\frac{\partial k}{\partial x} \tag{10}$$

c) Eddy Viscosity Definition (SST)

$$\mu_t=\frac{\rho k}{\max\left(\omega, F_2 S\right)};S=\sqrt{S_{ij}S_{ij}} \tag{11}$$

S: It is a strain rate magnitude

d) Blending Functions

The SST model employs blending functions F_1 and F_2 to smoothly transition between k–ω (near-wall) and k–ε (free-stream) behavior:

- $F_1 \rightarrow 1$: Near-wall region
- $F_1 \rightarrow 0$: Free-stream region

e) Production term

$$P_k=\min\left(\tau_{ij}\frac{\partial u_i}{\partial x_j},10\beta^*\rho k\omega\right) \tag{12}$$

3.2.4 Thermo-physical Modelling

a) Dynamic Viscosity (Sutherland's Law)

$$\mu=\mu_0\left(\frac{T}{T_0}\right)^{3/2}\frac{T_0+S}{T+S} \tag{13}$$

b) Effective Thermal Capacity

$$k_{eff}=\frac{\mu C_p}{P_r}+\frac{\mu_t C_p}{P_{r_t}} \tag{14}$$

c) Heat Flux

$$q_i=-k_{eff}\frac{\partial T}{\partial x_i} \tag{15}$$

4. GRID GENERATION

A structured grid is generated around the multi-row disk inlet. The grid is refined near the disks to capture the detailed shock and boundary layer interactions. The entire domain and the magnified image of the interior of the cavity are shown in Figure 8. Meshing over the STD model is shown in Figure 9.

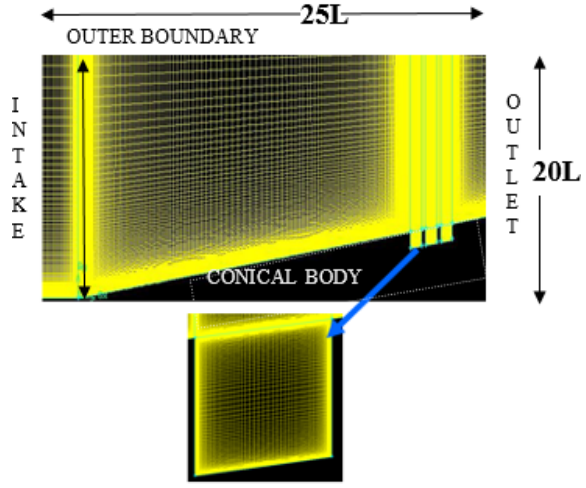

Figure 8: Mesh of the computational domain

The intake and the upper domain boundary have been specified by pressure far-field boundary condition. The cavity structure is specified with no-slip wall boun–

dary conditions, and the domain outlet is specified with pressure outlet. The conical part is considered as Sym–metry boundary condition. Grid points are clustered near the wall to capture steep gradients in the boundary layer. Clustering the grid near the cavity edges (both leading and trailing) helps resolve shock impingement and interaction with the shear layer.

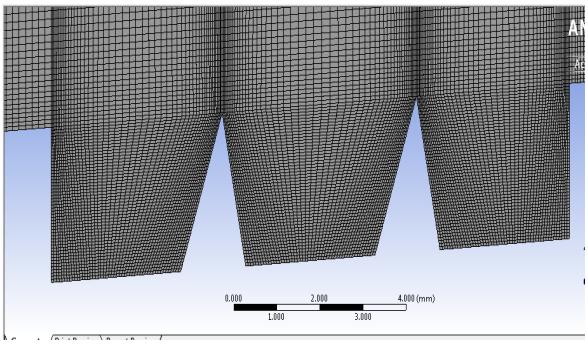

Figure 9: Meshing over the STD model

The dimensionless wall distance y^+has been given the priority to estimate the first cell distance from the wall. Detailed calculations have been undertaken based on the formula given below to systematically determine the grid spacing based on near-wall resolution requirements.

$$y^+ = \frac{y \cdot u_\tau}{\vartheta}$$
$$u_\tau = \sqrt{\frac{\tau_w}{\rho}} \qquad (16)$$
$$\tau_w = \frac{1}{2}\rho U^2 C_f$$

Value of $C_f$is estimated from the empirical relations which are widely available in the literature. In the current case it is estimated to be around 0.0037. The wall y^+ is taken to be 1 as reported in the multiple literatures. Further calculation based on the above for–mula and the experimental and the numerical data pro–vides the first cell height of approximately 1.6 microns.

Once the first cell height is obtained, Grid sensitivity tests have been undertaken to ensure that further refine–ment of the Grid does not significantly affect the results.

The total length of the simulation domain is taken as 25Lx20L. It has been obtained after multiple iterations to assure that shock structure is captured properly.

5. NUMERICAL SET-UP &VALIDATION

Numerical model validation has been undertaken based on the experimental data reported by Kobayashi et al. [24] on the MRDID. They reported the C_D values on the Type 2 and Type 3 MRD models. Complete details on the Type 2 and Type 3 models can be found in the same paper. Here C_D value has been validated through the numerical simulation. Type 1, Type 2 and Type 3 cor–responds to geometric variations of the model shown in Figure 3, and that the detailed geometrical parameters for all three configurations are provided in reference [14]. Two different types of meshing have been used – Coarse mesh and Fine mesh. Coarse mesh has 2,85,000 grid points and the Fine mesh has 5,50,000 grid points. Table 2 and 3 presents the numerical validation under–taken in reference to the experimental data published by Kobayashi et al. [24] and the deviation in the results for both the fine mesh and the coarse mech respectively.

Table 1. Cell counts for different Grid Types

Sl. No.	Mesh type	Cell Count
1	Coarse	285,000
2	Fine	550,000

Table 2. Grid validation with Fine mesh

MESH TYPE	**C_D Values**		
FINE MESH	**TYPE 1**	**TYPE 2**	**TYPE 3**
REFERENCE DATA [24]	0.076	0.08764	0.1035
Numerical data	0.07854	0.0863	0.1026
ERROR%	**3.34**	**1.52**	**0.87**

Table 3. Grid validation with coarse mesh

MESH TYPE	**C_D Values**		
COARSE MESH	**TYPE 1**	**TYPE 2**	**TYPE 3**
REFERENCE DATA [24]	0.076	0.08764	0.1035
Numerical data	0.07878	0.0838	0.1021
ERROR %	**3.658**	**4.38**	**1.35**

Above data shows the close proximity of the Expe–rimental data and the numerical data. However, for the better accuracy we have used Fine Mesh for further simulations. Further details on Type 1, Type 2 and Type 3 experimental models and the simulation models can be obtained in the paper by Sinha et al. [14].

Further numerical model and the Turbulence model validation have been undertaken with the Experimental results reported by Mohri and Hillier. Surface Pressure plot against the wetted cavity length has been compared as shown in Figure 10 and a good agreement has been found. Numerical data Presented by Gholap et al. [27] and Tembhurnikar et al. [28]. Further validation has been done based on the work of Milicev [29] and Dam–ljanović et al. [30]. The off-design performance of the model in the wind tunnel has been studied based on the work of Damljanović et al. [31].

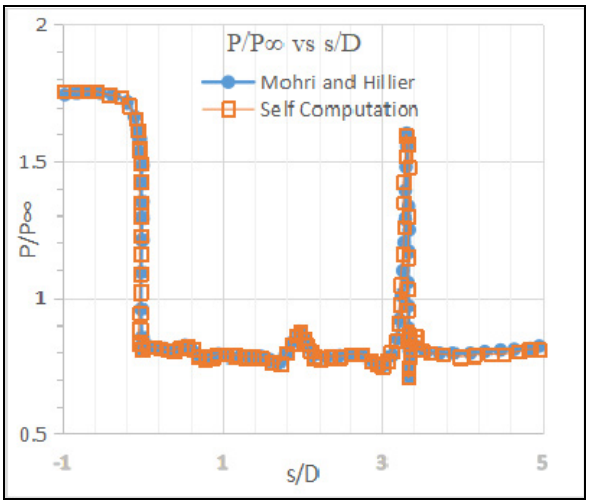

Figure 10. Solver validation graph depicting the plot of non-dimensionalized Pressure (P/P∞) vs wetted length (s/D)

During the simulation, the residuals of continuity, energy and turbulent kinetic energy were monitored. In

addition, the convergence history for drag was also mo–nitored during the entire solution period. Results were analyzed only when it was ascertained that the residuals have converged to the order of 10^{-5}.

Table 2 and 3 and Figure 10 clearly indicates that the discretization method and the grid generated for the analysis has good agreement with the numerical and the experimental reference data. So, further analysis has been undertaken with the Fine mesh and the solver data provided below.

Table 4. Solver Set-up

Scheme/parameters	Type/quantities
Solver precision	Double precision
Solver type	Density-based implicit, steady state
RANS	k-ω SST (2 PDE model)
Inviscid flux scheme	Roe flux-difference splitting scheme
Spatial discretization	Second-order upwind scheme
Gradient evaluation	Least squares cell-based

6. EXPERIMENTAL SET-UP

Experimental studies of FTD and STD models as shown in Figure 6 and 7 have been conducted at Supersonic Wind tunnel facility available at SRM University Chennai, India at Mach 2. The dimension of themodels is completely based on the test section of the supersonic wind tunnel. Both the models have maximum length of 90mm and maximum diameter of 12.63 mm. As the blockage ratio of the wind tunnel is 10% and the area of the test section is 100 square centimetre so we have given the maximum area of the test piece to be 5 square centimetre. The maximum area of our model is 1.246 square centimetre and the attachment is of screw and nut bolt. The maximum allowable length of the models, including the M15x1.5 threaded screw section, shall not exceed 130 mm.. The model is made-up of mild steel keeping in mind the manufacturing part as it leaves a very edgy design and breakage of the design is possible while manufacturing.All the models have the L/D ratio of the cavity as 1. Due to the small size of the model only a single static pressure probe is placed at the rear wall of the model.Both the FTD and STD models have similar maximum diameter and maximum length as mentioned above. Blockage ratio mentioned above is the ratio of the projected frontal area of the model and the cross-section of the test-section.

Multiple experimental runs were conducted, beginning with the FTD model to collect qualitative data through Schlieren optical flow visualization met–hod and quantitative data through static testing, as reported through Figure 11, 12 and Figure 15 respec–tively,followed by identical testing of the STD models to enable direct comparison.

7. RESULTS AND DISCUSSION: ANALYSIS OF THE EFFECT OF DISK GEOMETRY

Figure 11 and 12 shows the comparison, using the axi–symmetric 2D view for both the experimental and computational analysis of MRD device with flat tip and sharp tip disks forming the cavity of L/D=1. Both the model contains two disks. Computation and experimen–tations have properly captured the expansion waves and oblique shocks at thestart of the cavity, on the disks and at the rear of the cavity.

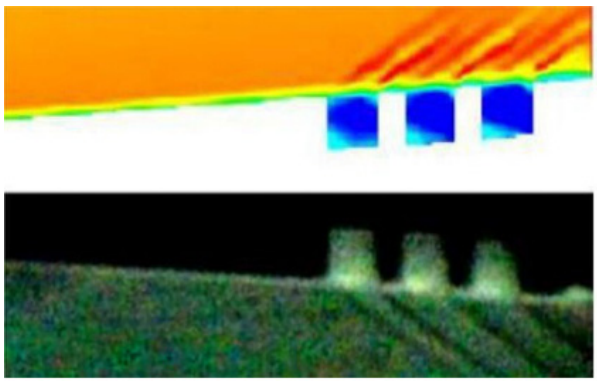

Figure 11. Comparison of the Numerical and the experimental shock structure for FTD

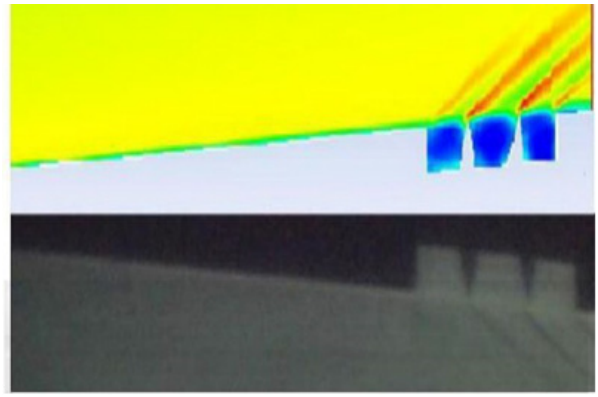

Figure 12. Comparison of the Numerical and the experimental shock structure for STD

Both the figures have captured the shock structures properly as per the physics of the cavity flow. Mag–nified vortical structure inside the cavity is shown in Figure 13.

Single vortical structure as shown in Figure 13 and 14 also validates the physics of the cavity of L/D=1.

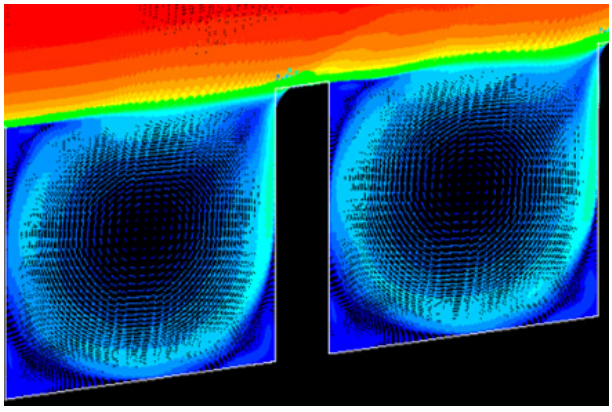

Figure 13. Single Vortical structure inside the cavity for FTD

Static pressure distribution over the wetted length of the 1st cavity shows the significant variation in the pre–ssure peak on the rear wall of the cavity. Peak pressure on the FTD is higher than the STD.

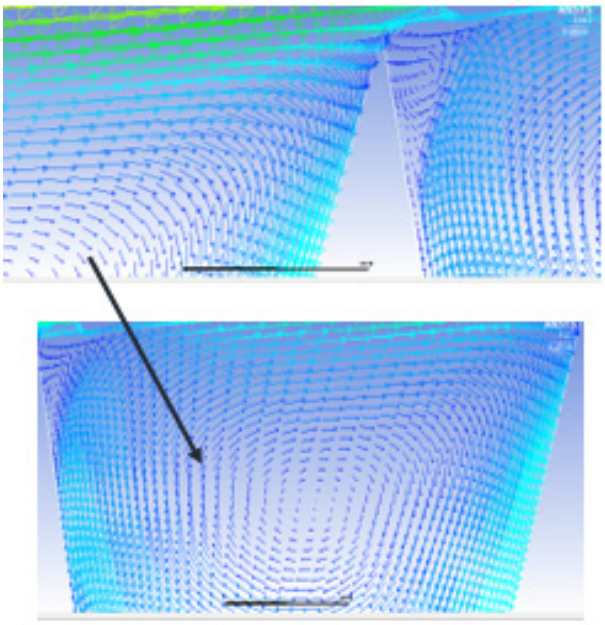

Figure 14. Single Vortical structure inside the cavity for STD

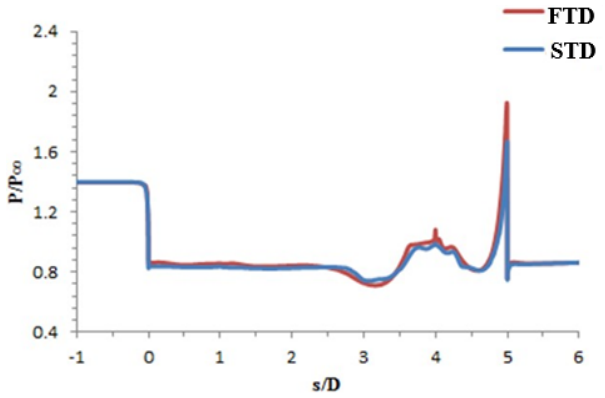

Figure 15. Comparison of wetted pressure distribution for FTD and STD

Detailed quantitativeoutcome of the numerical simulations on the cavities for both the cases is reported in Table 5. Comparative parameters used are - Peak P/P∞, Compression Ratio and Drag Coefficient. Compression ratio across shock waves was quantified using static pressure ratios across the shock waves, derived from pressure measurements. Experimentally, Compression ratio measurement has been avoided to eliminate any chances of local shock wave and flow disruptions caused due to intrusive pressure probs.High peak pressure in case of FTD as compared to STD is attributed to the local stagnation zone inside the FTD formed on the rear wall. In case of STD, the rear wall stagnation shock is formed on the slanted wall, which reduces its severity. Higher Stagnation zone creates better compression at the same time. FTD tends to generate higher drag due to increased frontal area and resistance as the flat surface interacts with the flow.

Table 5. Comparative chart for FTD and STD

Type of Disk	Peak P/P_∞	Compression ratio	Drag Coefficient
FTD	**1.824**	**1.530**	**0.016**
STD	**1.715**	**1.146**	**0.012**

Table 6. Comparative chart for FTD and STD simulated data against the experimental data.

Type of Disk	Peak P/P_∞ (Numerical)	PeakP/ P_∞ (Experimental)
FTD	**1.824**	**1.91**
STD	**1.715**	**1.77**

The above data provides higher P/P_∞ captured expe–rimentally. Such deviations could occur because of the following factors:

- Surface roughness and manufacturing imperfections
- Support/mounting interference

These increase local stagnation pressure and streng–then the oblique shock, producing higher peak P/P_∞.

8. EFFECT OF DIFFERENT OTHER DISK SHAPES

As a part of the analysis of disk shape, two other diffe–rent kind of disks have been developedby modifying the Flat Tip Disk(FTD)and tested numerically. First one is called Rear Chamfered tip disk (RCTD). It is designed by modifying the trailing tip of the FTD by chamfering and then smoothen to provide the smooth relaxation to the flow over the disk. Figure 16 shows the RCTD. Chamfering has been done with 5mm radius on the rear part. Second one is called Front Chamfered Tip Disk (FCTD). It is shown in Figure 17.

FCTD is formed by modifying the Front tip of the FTD by providing 45° slant from the rear tip to the front tip. Dimension of both FCTD and RCTD similar to that of the FTD.

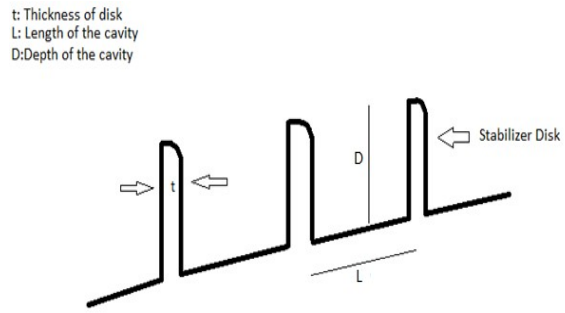

Figure 16. CAD model of RCTD

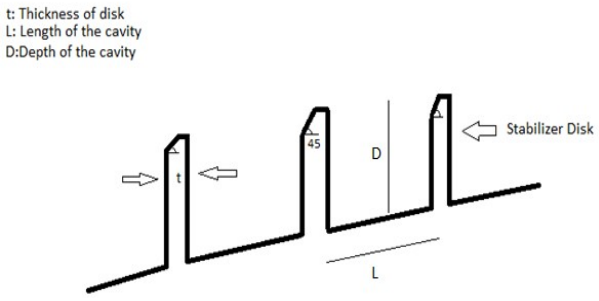

Figure 17. CAD model of FCTD

These geometric changes primarily influence the shock formation mechanism, separation behavior, and local stagnation intensity around the disk.

8.1 Rear chamfered tip disk (RCTD)

In the baseline FTD, the sharp rear edge causes:

- Sudden flow expansion

- Large recirculation bubble behind the disk
- Strong recompression shock interaction with the shear layer
- Low base pressure and enhanced pressure drag

Introducing a 5 mm radius rear chamfer with smooth blendingchanges this behavior fundamentally. Detailed modifications due to rear chamfering is tabulated below:

Table 7. Flow Physics Change

Feature	FTD	RCTD
Flow expansion	Sudden	Gradual
Wake region	Large recirculation	Reduced wake size
Base pressure	Low	Increased
Recompression shock	Strong	Weaker
Shear layer interaction	Intense	Reduced

8.1.1 Effect on P/P_∞

The rear chamfer does not significantly affect the pri–mary stagnation peak at the front face, but it reduces se–condary pressure rise caused by wake–shock interaction.

Peak pressure ratio obtained in RCTDis reduced by 5% compared to FTD.

The reduction arises primarily due to increased base pressure and weakening of wake-induced recompression shocks, which lower the secondary pressure rise in the downstream region. The front stagnation pressure remains largely unaffected, resulting in a modest overall reduction in peak P/P_∞.

8.2 Front Chamfered Tip Disk (FCTD)

In the baseline FTD, the sharp front edge behaves as a bluff obstruction, creating:

- Detached bow shock
- Immediate stagnation
- Strong pressure spike
- Early boundary layer separation

By chamfering the front tip, the disk front face becomes an inclined compression ramp.

Table 8. Flow Physics Change

Feature	FTD	FCTD
Shock strength	Strong	Weaker
Stagnation	Abrupt	Gradual compression
Separation	Immediate	Delayed

8.2.1 Effect on P/P_∞

Since the maximum pressure originates at the upstream face, modifying this region has the largest impact.

Peak pressure ratio in FCTDis reduced by 12% compared to FTD.

This is significantly larger than RCTDbecause the stagnation mechanism itself is altered.

9. CONCLUSION

This study systematically investigated the influence of disk edge geometry on the flow physics, pressure characteristics, and shock structure of a multi-row disk inlet device (MRDID) operating at Mach 2 within the open cavity regime ($L/D = 1$).

The numerical model was rigorously validated against published experimental data from Kobayashi et al., Mohri and Hillier, and additional benchmark studies, demon–strating strong agreement in drag prediction and cavity pressure distribution. Further validation aga–inst in-house experimental measurements confirmed that the solver setup, grid resolution (, and boundary conditions were adequate to $y^+ \approx 1$) capture the essential physics of supersonic cavity flow and shock interactions.

Comparison between the flat tip disk (FTD) and sharp tip disk (STD) revealed that disk geometry stron–gly governs the formation and location of stagnation zones inside the cavity. The FTD generates a stronger stagnation region at the rear wall of the cavity.

The consistent trend of slightly higher experimental peak pressures (3–5% above CFD) was attributed to real-flow effects such as surface roughness, mounting inter–ference, and enhanced shock–boundary layer interaction that are inherently under-resolved in RANS simulations.

The study demonstrates that disk edge shaping acts as an effective passive shock control mechanism in MRDID configurations. Rear chamfering improves wake recovery and pressure relaxation, while front chamfering directly reduces stagnation strength and shock severity. Among all configurations, the front chamfered tip disk (FCTD) provides the most favorable balance between compression, reduced pressure peaks, and lower drag.

From an inlet design perspective, this work high–lights that passive geometric optimization of disk edges can be as influential as modifying disk spacing or cavity aspect ratio. The findings provide a practical design guideline for MRDID-based supersonic intakes where improved pressure recovery, reduced drag, and cont–rolled shock structure are desired without intro–ducing mechanical complexity.

Further analysis into the chamfer-modified Disk Shape will be carried out into the next version of the paper otherwise the length of the current paper would increase substantially.

ACKNOWLEDGMENT

The authors would like to thank all the faculty and staff members of Amity Institute of Aerospace Engineering, who provided valuable feedback during this research.

REFERENCES

[1] Farhani, M, and Mahdavi, M.M: A proposed design method for supersonic inlet to improve performance parameters, Aerospace Science and Technology, Vol. 91, August 2019, pp. 583-592.

[2] Wu, Z. et al.: Influence of the shock wave-turbu–lence interaction on the swirl distortion in hyper–sonic inlet, Adv. Aerodyn. Vol. 6, No. 23, 2024.

[3] He-xia Huang et al..: A review of the shock-dominated flow in a hypersonic inlet/isolator, Progress in Aerospace Sciences, Vol. 143, 2023

[4] Lianjie Yue, Xu Zhang, Qifan Zhang, et al.: Research progress on High-Mach-number scramjet

engine technologies, Chinese Journal of Theoretical and Applied Mechanics, Vol. 54 No. 2,pp. 263–288 2022.

[5] Ommi, F., Farajpour Khanaposhtani, V., Agha Seyed Mirzabozorg, M., Nekoufar, K..: A new app–roach for supersonic diffuser design, Journal of Applied Sciences Research, Vol. 6, No. 5. pp. 401-414, 2010.

[6] Sinha, J., Singh, S., Prakash, O. and Panchal, D.: Design Optimization of a Multi Row Disk Inlet Device with an Optimum Nose Cone Angle, FME Transactions, Vol. 51, No. 1, pp. 23-30, 2023.

[7] Khobragade N, Unnikrishnan S, Kumar R.: Flow instabilities and impact of ramp–isolator junction on shock–boundary-layer interactions in a super–sonic intake, Journal of Fluid Mechanics, 2022.

[8] Sabnis, K., Babinsky, H.: A review of three-dimen–sional shock wave–boundary-layer interactions, Progress in Aerospace Sciences, Vol. 143, 2023.

[9] Zhuang, N., Alvi, F. S., Alkislar, M. B., Shih, C.: Supersonic cavity flows and their control, AIAA Journal, Vol. 44, No. 9, 2006.

[10] Mohri, K., Hillier, R.: Computational and experi–mental study of supersonic flow over axisymmetric cavities,Shock Waves, Vol. 21, No. 3, pp. 175–191, 2011.

[11] Kobayashi, H., Maru, Y. Hongoh, M., Takeuchi, S., Okai, K., Kojima, T.: Study on variable-shape supersonic inlets and missiles with MRD device, ActaAstronautica Vol. 61, pp. 978 –988. 2007.

[12] Kobayashi, H., Kojima, T., Okai, K. and Maru, Y.: Study of Supersonic Cavity Flow in Advanced Va–riable Geometry Inlet, *55th International Astro–nautical Congress* Vancouver, Canada. 2004.

[13] Sinha, J., Kumar, N., Kaul,A.: Study of Supersonic Flow around Tandem Cavities, International Jour–nal of Mathematics Trends and Technology, Vol. 48, No. 5, pp.292-296, 2017.

[14] Sinha, J., Arora, K., Prakash, O., Bandopadhyay S., Saha, P., Bhattacharya, A.: Analysis of multi row disk inlet device in supersonic flow condition, *21st Annual CFD Symposium*, August 2019, Bangalore, India.

[15] Jeyakumar, S., Assis, S. M., Jayaraman, K..: Shape effects of a single axisymmetric cavity in a circular duct on flow-induced acoustic oscillations, Aero–space Science and Technology, Vol. 67, pp.181-192, 2017.

[16] Prasath M., Desikan, S.L.N., Vaidyanathan, A.: Oscillatory characteristics of cavities in supersonic flow, European Journal of Mechanics-B/Fluids, Vol. 98, pp. 224-237, 2023.

[17] Gaitonde, V.D.: Progress in shock wave/boundary layer interactions,Progress in Aerospace Scien–ces,Vol. 72, pp. 80-99, 2015.

[18] Seyed, A.A.M.: A computational investigation of shock wave train in diverse duct geometries using machine learning-adopted k-ω turbulence model, ActaAstronautica, Vol. 217, pp. 27–36, 2024.

[19] Liu, C.L., Gao, H.W., Zhang, X.B.: Multi-objective aerodynamic optimization of an axisymmetric variable-geometry inlet with a Mach 5 design point, Aerospace Science and Technology, Vol. 136, 108189, 2023.

[20] Sinha, J., Singh, S., Prakash, O., Panchal, D.: Passive flow modification over the Supersonic and the Hypersonic air-intake system using Bleed**,** FME Transactions, Vol. 51, No. 2, pp. 329-337, 2023.

[21] Chen, H., Tan, H.J.: Buzz flow diversity in a super–sonic inlet ingesting strong shear layers. Aerospace Science and Technology,*Vol. 95*, 105471, 2019.

[22] Szulc, O., Doerffer, P., Flaszynski, P., Suresh, T.: Numerical modelling of shock wave-boundary layer interaction control by passive wall ventilation, Computers & Fluids, Vol. 200, 104435, 2020.

[23] Tam, C. K. W., Block, P. J.: On the tones and pres–sure oscillations induced by flow over rectangular cavities. Journal of Fluid Mechanics, Vol. 548, pp. 315–346, 2006.

[24] Fang, Y., Sun, D., Dong, X., Sun, X.: Effects of Inlet Swirl Distortion on a Multi-Stage Compressor with Inlet Guide Vanes and Stall Margin Enhan–cement Method, Aerospace, Vol. 10, No. 2, 2023.

[25] Ferrero, A.: Control of a supersonic inlet in off-design conditions with plasma actuators and bleed, Aerospace, Vol. 7, No.3, 32, 2020.

[26] Sinha, J., Singh, S., Prakash, O., and Panchal, D.: Analysis of supersonic intake design for multi-row disk intake device under varying Mach numbers and angle of attacks, FME Transactions, Vol. 53, pp. 38–50, 2025.

[27] Gholap, T.B., Salokhe, R.V., Ghadage, G.V., Mane S.V., and Sahoo, D.: Aerodynamic Analysis of an AK-47 Bullet Moving at Mach 2.0 in close pro–ximity to the Ground, FME Transactions, Vol. 50, No. 2, pp. 369-381, 2022.

[28] Tembhurnikar, P.V., Jadhav, A.T., Sahoo, D.: Effect of Intermediate Aerodisk Mounted Sharp Tip Spike on the Drag Reduction over a Hemispherical Body at Mach 2.0, FME Transactions, Vol. 48, pp. 779-786, 2020.

[29] Milićev, SS.: An Experimental Study of the Influ–ence of Spike in Supersonic and Transonic Flows Past a Hemispheric Body, FME Transactions, Vol. 50, No. 1, PP. pp. 24-31, 2022.

[30] Damljanović, D., Vuković, D., Ocokoljić, G., Rašuo, B.: Convergence of Transonic Wind Tunnel Test Results of the AGARD-B Standard Model, FME Transactions, Vol. 48, No. 4, pp. 761-769, 2020.

[31] Damljanović, D., Vuković, Đ., Ocokoljić, G., Ilić B., Rašuo, B.: Wind Tunnel Testing of ONERAM, AGARD-B and HB-2 Standard Models at Off-Design Conditions, Aerospace, Vol. 8, No. 10, 275, 22 Sep. 2021.

Acronyms

STD	Sharp Tip Disk
FTD	Flat Tip Disk

RANS	Reynold's Average Naviers Stokes
MUSCL	Monotonic Upstream-Centered Scheme for Conservation Laws
L/D	Length-to-Depth Ratio
SST	Shear Stress Transport
P/P_∞	Ratio of Local pressure and Free stream pressure
M	Mach number
MRDID	Multi Row Disk Inlet Device
C_D	Drag coefficient
RCTD	Rear Chamfered Tip Disk
FCTD	Front Chamfered Tip Disk
C_f	Friction coefficient
k	Turbulent kinetic energy
ω	Specific dissipation rate
ε	Turbulent dissipation rate
R-K method	Runge-Kutta Method
CFL	Courant–Friedrichs–Lewy
CAD	Computer Aided Design
CFD	Computational Fluid Dynamics

NOMECLATURE/ABBREVIATIONS

ρ	Fluid density
u_i	Velocity component in i^{th} direction
u_j	Velocity component in j^{th} direction
x_i	Spatial coordinate in in i^{th} direction
t	Time
p	Static pressure
E	Total energy per unit mass
h	Static entalpy
T	Temperature
R	Specific gas constant
τ_{ij}	Viscous stress tensor
δ_{ij}	Kronecker delta
μ	Dynamic (laminar) viscosity
μ_t	Turbulent (eddy) viscosity
k	Turbulent kinetic energy
ω	Specific dissipation rate
ε	Turbulent dissipation rate (not used in SST, reference only)
P_k	Production term of turbulent kinetic energy
F_1, F_2	SST blending functions
a_1	SST model constant (viscosity limiter)
S	Magnitude of strain rate
σ_k	Turbulent Prandtl number for (k)
σ_ω	Turbulent Prandtl number for (\omega)
$\sigma_{\omega 2}$	Cross-diffusion constant
α	Model coefficient
β	Model coefficient
β^*	Model coefficient
k_{eff}	Effective thermal conductivity
q_i	Heat flux vector
C_p	Specific heat at constant pressure
Pr	Molecular Prandtl number
Pr_t	Turbulent Prandtl number
$u_i'u_j'$	Reynolds stress components
$\overline{u_i'u_j'}$	Time-averaged Reynolds stress

ОПТИМИЗАЦИЈА ПЕРФОРМАНСИ УЛАЗНОГ ОТВОРА MRD-А КРОЗ МОДИФИКАЦИЈУ ГЕОМЕТРИЈЕ ДИСКА ПРИ РЕЖИМУ НАДЗВУЧНОГ ПРОТОКА

Ј. Сихна, С. Синг, О. Пракаш

Ова студија истражује утицај геометрије ивице диска на физику протока и карактеристике притиска вишередног диска за улаз (MRDID) који ради на Маху 2 у режиму отворене шупљине (L/D = 1). Детаљна параметарска анализа је спроведена коришћењем 2D осносиметричних RANS симулација са SST k-ω моделом турбуленције и MUSCL дискретизацијом другог реда, уз подршку експеримента у надзвучном аеротунелу ради валидације. Две основне геометрије, диск са равним врхом (FTD) и диск са оштрим врхом (STD), су испитане како би се разумела улога стагнације задњег зида и интеракције удара шупљине. Резултати показују да FTD производи веће односе вршних притиска, компресије и отпора због јаке зоне стагнације на задњем зиду шупљине, док STD смањује тежину стагнације кроз своју нагнуту површину. Да би се истражила пасивна контрола протока, уведене су две модификоване геометрије - диск са задњим закошеним врхом (RCTD) и диск са предњим закошеним врхом (FCTD). Задње закошење побољшава опоравак од таласа и смањује рекомпресионе ударе, док предње закошење трансформише одвојени прамчани ударни ток у причвршћени коси ударни ток, значајно смањујући вршни притисак. Студија утврђује обликовање ивице диска као критични параметар пасивног дизајна за оптимизацију перформанси улазног отвора MRD-а.